

Temperature measurements of magnesium- and aluminum-based flares

Claudiu Lăzăroaie · Sorin Eșanu · Ciprian Său ·
Răzvan Petre · Petrișor-Zamora Iordache ·
Georgios Staikos · Traian Rotariu · Teodora Zecheru

Received: 30 March 2013 / Accepted: 12 August 2013 / Published online: 5 September 2013
© Akadémiai Kiadó, Budapest, Hungary 2013

Abstract Experimental researches were performed in order to determine the combustion temperatures and the visible and infrared screening performances of two pyrotechnic compositions used in decoy flare systems. Morpho-structural and morphochemical analyses of the combustion solid products have been correlated with the combustion temperature. For the experimental studies, visible and infrared thermography have been employed, together with dedicated software. The comparative measurements indicated that the thermovision camera enables the acquisition of more accurate results versus the optical pyrometer in terms of data processing, and that the aluminum/polyhalogenated compounds–compositions present visible and infrared screening performances superior to those based on magnesium/polyhalogenated compounds.

Keywords Aerosols · Combustion temperature · Infrared thermography · Pyrometer · Pyrotechnics

Introduction

The temperature is one of the parameters of state frequently measured in industry, research, and current life, while

thermal imaging is one of the technologies of essential importance for the military and security sector. Previous theoretical and experimental studies have demonstrated that the main principle for conceiving pyrotechnics is the obtainment of an optimum pyrotechnical effect: light, smoke, sound, etc. More, there is a direct relationship between the chemical composition and the combustion temperature of a pyrotechnic composition and its destination [1–4]. Some figures from literature are given in Table 1 [4, 5].

Therefore, a compelling determination of the combustion temperature of pyrotechnic compositions is mandatory, taking into account that its high gradient influences the compositions performances, and the obtainment of pyrotechnical effects, such as light emission in different wavelength ranges, visible and infrared concealing and screening, metal melting, aerosols generation, etc. In other situations, a lower combustion temperature is appropriate, either to protect the organic compounds incorporated in the pyrotechnic composition (dyes for colored smoke compositions, tear agents for irritating and lachrymator aerosol formulations, etc.), or to obtain low-temperature gaseous combustion products (gas-generators, airbags, and flame-retardant compositions), meanwhile considering the environment and the operational staff [3–18]. Thus, it offers a great utility to the operators, giving a new evaluation criterion on the existent pyrotechnical compositions and a real help in conceiving new formulations, specific to the pyrotechnical effects desired.

In order to evaluate whether the mixture corresponds to the target aimed, it is necessary to find the real values of the combustion temperature. Depending on the flame temperature, pyrotechnics have either high combustion temperature, $T_c > 2,200$ °C, or low combustion temperature, $T_c < 2,200$ °C. Organic fuel-based compositions belong to the second category, while metallic compositions belong to

C. Lăzăroaie · C. Său · R. Petre · P.-Z. Iordache ·
T. Zecheru (✉)
Scientific Research Center for CBRN Defense and Ecology,
225 Sos. Oltenitei, 041309 Bucharest, Romania
e-mail: teodora.zecheru@yahoo.com

S. Eșanu · T. Rotariu · T. Zecheru
Military Technical Academy, 81-83 Bd. George Cosbuc,
050141 Bucharest, Romania

G. Staikos
Faculty of Chemical Engineering, University of Patras,
265 04 Rio Patras, Greece

Table 1 Flame temperatures versus pyrotechnics destination [4, 5]

Pyrotechnics destination	Temperature/°C
Photography, illumination	2,500–3,500
Illumination, tracers	2,000–3,000
Incendiary (with oxidant)	2,000–3,500
Night signaling	1,200–2,000
Propergols	2,000–2,900
Smoke compositions	400–1,200

the first one, giving combustion temperatures of up to 4,000 °C [4].

Another important requirement regarding pyrotechnics' composition is to decrease their sensitivity and to increase their stability, but the utilization of different additives involves the modification of chemical and physical properties of the pyrotechnical system, meanwhile changing their ignition characteristics. Regarding the combustion temperature, it is obviously one of the main characteristics when considering flares and decoy compositions; its determination may be performed either through calculus or through measurement.

In case of pyrotechnics, actually it is almost impossible to predict through calculus the flares combustion temperature, due to the fact that specific data on the calorific capacities at high temperatures (especially over 1,500 °C) of the substances resulting from the reaction are not available. Melting and vaporizing latent heats are also unknown for a large number of reagents employed, or the precision given is rather poor. Moreover, the temperatures determined are nothing more than the upper thresholds (practically untouchable) due to thermal energy losses through convection, conduction, and radiation within the environment and, also, due to thermal losses during the reaction products dissociation processes.

However, the combustion temperature is not measured directly, but through the intermediary of thermocouples, optical pyrometers, or thermal cameras [1, 2, 4, 12, 19]. This temperature measurement is the subject of a lower number of theoretical and experimental studies as expected, due to the high cost of the equipment and the testing conditions required. Thus, the present study aimed at the experimental determination of two pyrotechnical flares performances, mainly the combustion temperatures and the evaluation of their screening capacity.

Materials and methods

Materials

Magnesium- and aluminum-based compositions are mainly used in infrared screening due to the large quantity of

Table 2 Composition of the pyrotechnical flares tested

No.	Composition	Reagents	Ratio in the mixture/%
1	Magnesium-based pyrotechnical flare (PF-Mg)	Magnesium	30
		Polytetrafluoroethylene	60
		Iditol	10
2	Aluminum-based pyrotechnical flare (PF-Al)	Aluminum	30
		Polytetrafluoroethylene	60
		Iditol	10

energy emitted in comparison to other pyrotechnical mixtures, their low hygroscopicity and low dependence of burning rate on pressure and temperature, and safety during the fabrication process [5, 8–21]. The addition of a polymeric binder allows the composition to be processed easily, and provides good mechanical properties while maintaining the homogeneity of the mixture [22] and a good protection against the environmental agents conducting to magnesium and aluminum oxidation. The compositions considered (Table 2) present a good thermal stability and compatibility with the vast majority of the materials used in pyrotechnics [23].

Determination of the combustion temperature

The equipment and the methods used for the combustion temperatures determination were based on the optical radiation transmittance variation principles through gaseous environments containing the aerosol suspension, depending on the wavelength, the environment, and the aerosol characteristics. The data have been analyzed based on the thermographs obtained from: a ThermaCAM S45 thermovision camera (Inframetrics), ± 2 % precision, 0.1 °C resolution, in the range $-40 \dots +1,700$ °C and the spectral range 8–12 μm (IR), with ThermaCAM Researcher Pro 2.8 SR-2 software for thermal analysis in real time; an optical pyrometer Ircan Ultimax UX-60P (Ircan Inc.) in the range 600–2,000 °C and the spectral range 8–12 μm , ± 1 % precision, 1 °C resolution, with dedicated software for data analysis; ImageJ software for visible image analysis [24, 25].

The recording in the visible range has been performed with a Sony Camcorder HDR-CX210E, 25 \times optical zoom and 3072 \times 1728 maximum image resolution. The combustion temperature has been measured using both the thermovision camera and the optical pyrometer, placed at 2.5 m away from the combustion site. The equipment has been calibrated previous to use by the method described [1, 26, 27]. For all the data recorded, the emissivity has been set to 0.7 [28].

Determination of the maximum temperatures

The pyrometer software gave directly, during combustion, the maximum temperature recorded. ThermaCAM Researcher Pro 2.8 SR-2 software used for the analysis of the thermographs recorded by the thermal camera gave the color thermal mapping of the investigated compositions, maintaining the same temperature scale whatever the temperature range involved, and the temperature profiles for the selected areas. The data processing has conducted to the obtainment of the temperature profile, together with the aerosol cloud temperature distribution and the maximum temperatures.

ImageJ software has been used for the computation of the data recorded in visible range. The software has the option of transforming a color image in a gray-level image; every pixel of this image is attributed spatial coordinates and a gray level that varies between 0 and 255 (pixel intensities: black = 0 and white = 255), corresponding to the input signal. After the video-recording of the aerosol cloud, relevant images of their evolution during time have been frozen. The input data consisted in the selected area from the image chosen for investigation, and the output data have been the histograms describing the counts distribution versus the gray level, from 0 to 255. Before selecting the area of interest, the image has been scaled, establishing a relationship between the pixel number and a known dimension from the plan. Average pixel intensity (I_a) has been determined from the histogram. Further, the interest area has been selected from the aerosol print film sequence and it appeared as the highest value of I_a .

The temperature has been calculated knowing that the radiant exitance is the radiant power emitted per the projected area of a source, or:

$$L = E \cdot 4\pi \cdot d^2 \quad (1)$$

and considering the Stefan–Boltzmann law, which states that

$$L = A \cdot \sigma \cdot T^4, \quad (2)$$

where L is the combustion power (W), E is the radiant exitance (W m^{-2}), d is the distance between the receptor (the camera) and the combustion site (m), A is the radiated area (m^2), σ is 5.6705×10^{-8} ($\text{W m}^{-2} \text{K}^{-4}$), the Stefan–Boltzmann radiation constant, and T is the combustion temperature (K).

Further, the calibration equation obtained was: $E_{8-12} = -73.91 + 0.55 I_a$.

Determination of the screening performance

The screening performance is represented here by the capability of the pyrotechnic composition to obscure certain targets for a definite period of time. The screening

efficiency has been calculated as the ratio between the effective screening period of time and the total combustion time:

$$\eta_s = \frac{t_s}{t_c}, \quad (3)$$

where η_s is the screening efficiency (%), t_s is time of effective screening (s), t_c is time of combustion (s).

The effective screening period of time represents the time that the target is not observed by the receptor, in the present case—the thermal camera. The total combustion time is the total time of pyrotechnics functioning from ignition until complete consumption; it is determined through direct measurement.

Elemental and morphostructural analysis of the aerosols

Morphostructural investigations of the aerosols resulting from the pyrotechnics combustion have been performed using scanning electron microscopy (SEM) on a VEGA II LMU equipment, at a 3.5-nm resolution and 30 keV, coupled with a Bruker AXS X-ray spectrometer for Energy-Dispersive X-ray analysis (EDX). Combustion products from confined samples have been collected on double-sided adhesive carbon disks and analyzed attached to aluminum stubs.

Results and discussion

Temperature is the most important thermodynamic property, which determines the state of matter. It is also one of the physical properties that cannot be measured directly, but through another physical parameter. Temperature can be measured using a spot or a contactless measurement method of temperature distributions on the surface of the tested objects, or thermovision. The contactless temperature

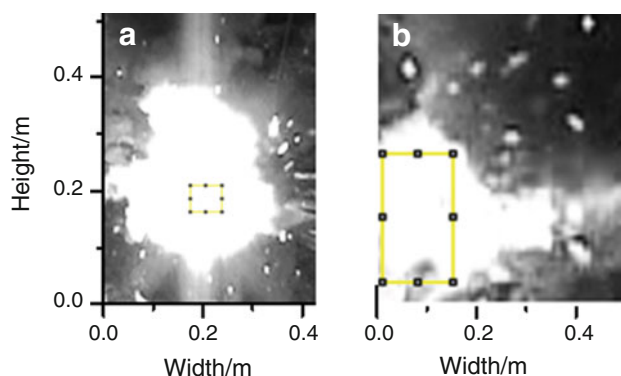
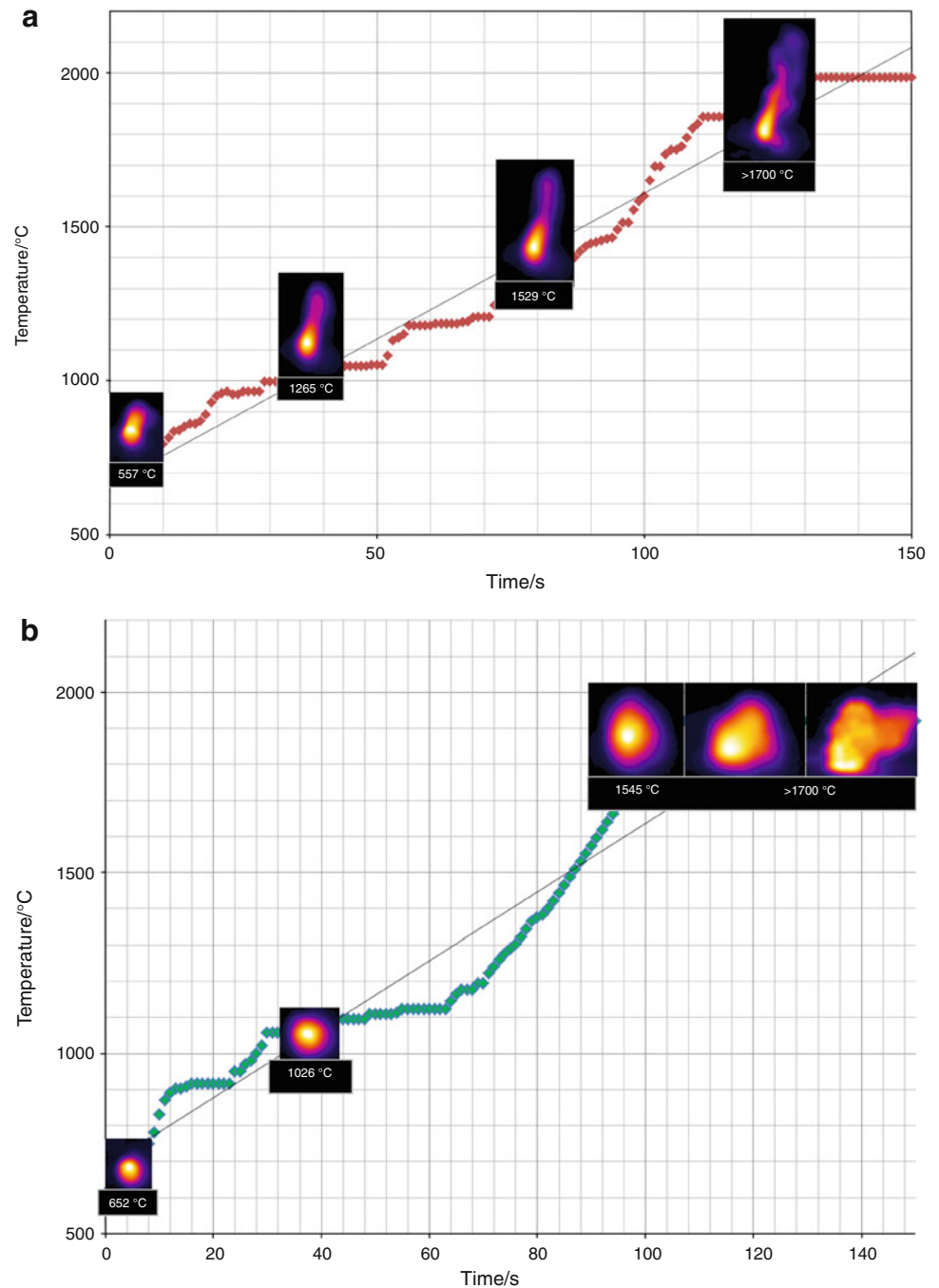


Fig. 1 Combustion of **a** PF–Mg; **b** PF–Al, and the selected areas at the maximum emission moment

Fig. 2 Pyrometer data and camera thermographs: **a** PF–Mg; **b** PF–Al



measurement is carried out using pyrometers or thermovision equipment.

Nowadays, there are thermal imaging sensors with suitable performance parameters. There are two different spectral wavelength ranges that provide thermal sensitivity: the medium-wave infrared band (MWIR), which covers the electromagnetic spectrum from 3 to 5 μm , and the long-wave infrared band (LWIR), which covers the wavelength spectrum from 8 to 12 μm . The two spectral bands differ substantially with respect to background flux, scene

characteristics, temperature contrast, and atmospheric transmission under various weather conditions. The latter technology is preferred both in terms of performances in fog, dust, and smoke conditions; higher immunity to atmospheric turbulence; and reduced sensitivity to solar glints and decoy flares (bright phenomena) recording, and equipment cost [1, 2, 26, 27, 29].

Thus, the results of temperature measurements obtained by means of an optical pyrometer have been compared with the results of a thermovision camera in the LWIR. The

Fig. 3 PF–Mg combustion thermograph: **a** image with emphasized saturation points; **b** raw thermal image

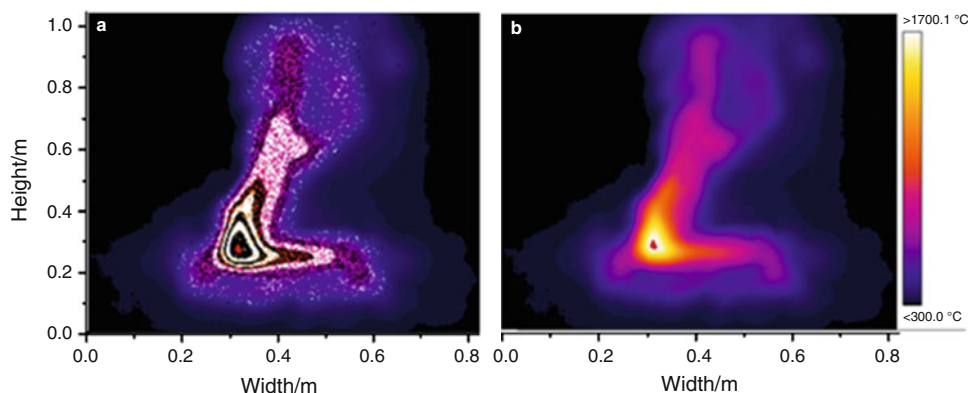
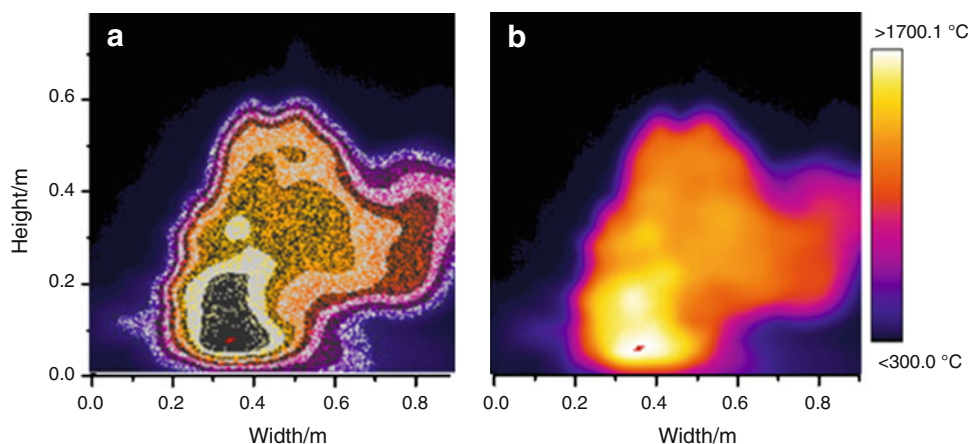


Fig. 4 PF–Al combustion thermograph: **a** image with emphasized saturation points; **b** raw thermal image



images captured during the combustion have been processed further using ImageJ (Fig. 1) and ThermoCAM software (Figs. 2, 3, 4).

Analysis in the visible range

In the visible range, the temperatures have been computed from the images using the Eqs. 1 and 2 above. ImageJ software has been used to analyze the images corresponding to the maximum emission moment of the PF–Mg (Fig. 1a) and PF–Al (Fig. 1b) composition. The results obtained for PF–Mg imply a temperature $T = 1,960\text{ }^\circ\text{C}$. Such a temperature has been expected in case of PF–Mg, which has also presented combustion temperatures at the maximum thresholds of the pyrometer and of the thermal camera.

The image corresponding to the moment of maximum emission during PF–Al combustion involves a calculated temperature $T = 1,697.6\text{ }^\circ\text{C}$.

The average maximum combustion temperatures, obtained using the pyrometer, are very similar for the two flares considered: for PF–Mg is $1,948\text{ }^\circ\text{C}$ and for PF–Al is $1,920\text{ }^\circ\text{C}$ (Fig. 2).

Infrared thermography

ThermoCAM Researcher Pro 2.8 SR-2 software has been used to perform both temperature recordings and profile analyses in the combustion area.

For PF–Mg (Fig. 3), the thermographs evaluation conducted to the determination of the maximum temperature, which was higher than $1,700\text{ }^\circ\text{C}$ (but not traceable with exactitude, due to the thermal camera construction limitations), in agreement with the results obtained using the pyrometer ($1,948\text{ }^\circ\text{C}$) and the bibliographic references for magnesium/polyhalogenated compounds-based pyrotechnical compositions [2, 3, 9, 11–13, 30].

Regarding PF–Al (Fig. 4), from the analyses performed using the camera software, the maximum temperature obtained has reached values $>1,700\text{ }^\circ\text{C}$, in agreement with the results estimated and the bibliographical references for aluminum-based pyrotechnics [2, 4, 10–12, 20]. Comparatively, the pyrometer determined a maximum temperature of $1,920\text{ }^\circ\text{C}$.

Also, the software provided the aerosol cloud temperature, ranging between $1,000$ and $>1,700\text{ }^\circ\text{C}$ for both the compositions considered during the study (Fig. 4). The histogram obtained from the data processing of Fig. 3 (Fig. 5a) shows that PF–Mg has a distribution of

temperatures ranging from 1,000 to >1,700 °C, mainly in the range 1,280–1,420 °C (30.2 % of the total amount), and 17.2 % in the moment of maximum emission (>1,700 °C). PF–Al temperature has an overall value higher than PF–Mg (Fig. 5b), being distributed in the range 1,140... >1,700 °C, and the main temperature ranging

between 1,420 and 1,560 °C, with 42.4 % and 31.8 % in the moment of maximum emission (>1,700 °C).

Screening performance

Screening performance has been determined in order to establish the pyrotechnics performances both in visible and infrared, using a human target. Ten samples from each composition have been tested and the data obtained using Eq. (3) conducted to the following results: the screening efficiency in visible has been calculated to be only 16 % in case of PF–Mg and 71.43 % in case of PF–Al, while in infrared it overpassed 90 % in both cases: 96 % for PF–Mg and 92.86 % for PF–Al.

Morphostructural and morphochemical analysis

In order to reveal the aerosols compactness and surface structure, detailed SEM and EDX investigations have been performed (Figs. 6, 7, 8, 9).

The main approach has been to acquire useful information for the understanding of aerosol morphologic distribution; the SEM has a good focus depth owing to differential emission of secondary electrons coming from the material phases. Besides, the EDX investigations allowed the identification of aerosol composition, through chemical mapping.

The particles dimensions were determined through SEM investigations (Fig. 7) and their estimated average values were correlated with the peaks found in the case of microsurface distribution. As Fig. 8 depicts, the microparticles present a wide distribution of their dimensions, mainly in the case of microspheres and roundness. For the

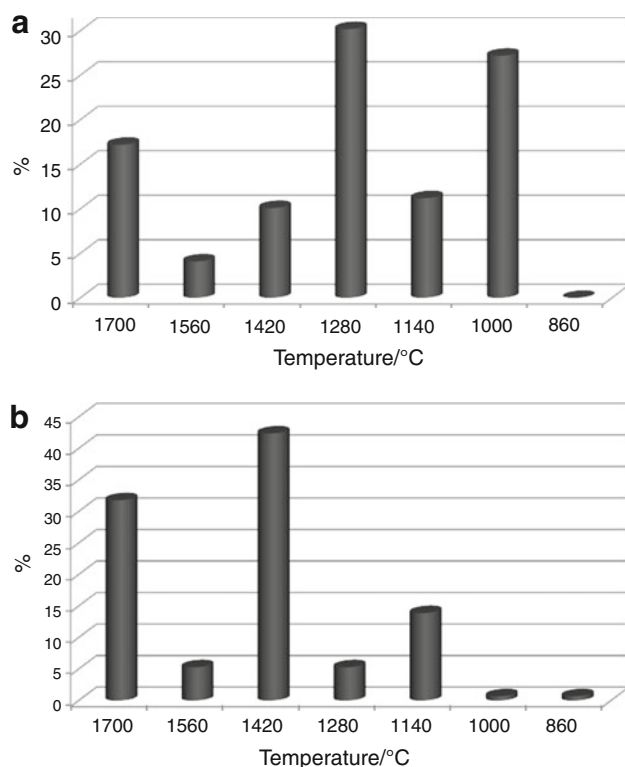
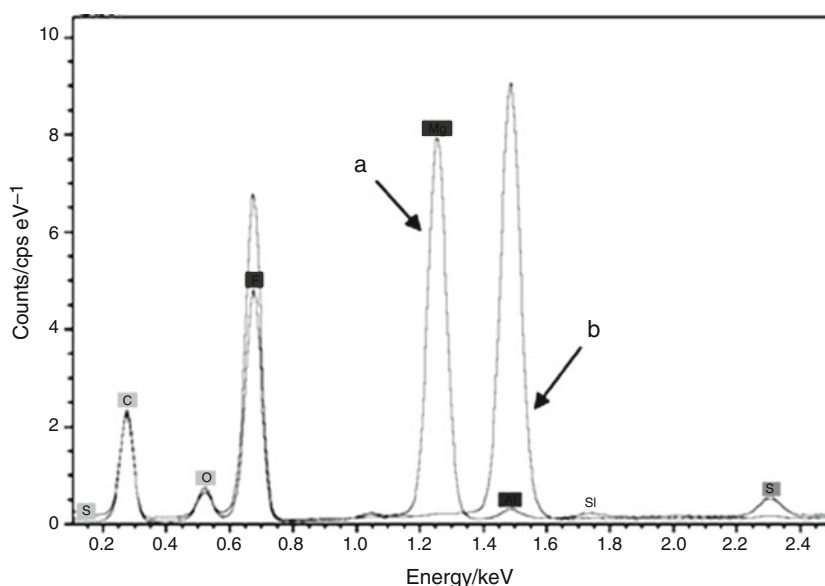


Fig. 5 Histograms corresponding to the aerosol temperature mapping: **a** PF–Mg; **b** PF–Al

Fig. 6 EDX spectra of *a* PF–Mg and *b* PF–Al combustion solid products



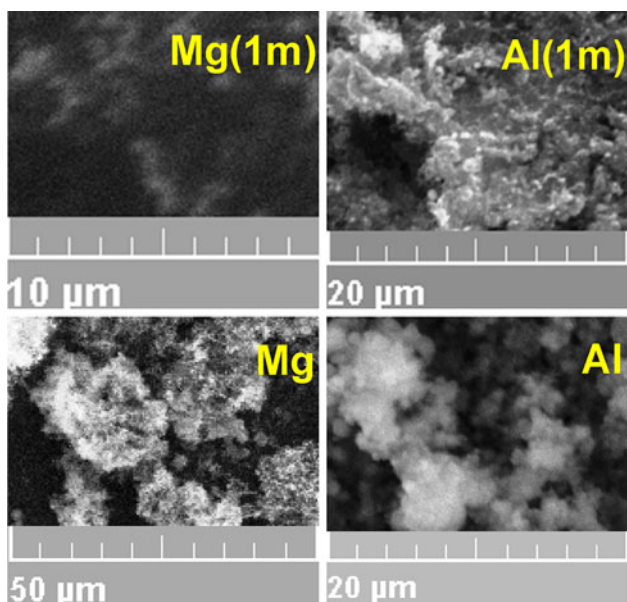


Fig. 7 SEM microphotographs for PF-Mg and PF-Al aerosol samples taken from the combustion site and from 1 m away

investigation of particles size distribution, as well as the range of size distribution, the method reported by Iordache et al. [31] was employed. Each SEM microphotograph was elementary segmented in order to acquire the numerical values belonging to the microspheres of SEM-recognized microparticles, as well as to evaluate their corresponding roundness. Subsequently, these values were plotted and their graphs are given in Fig. 8.

EDX results proved that MgO, elemental C, and MgF₂ are the main solid products resulting from the combustion of PF-Mg (Fig. 6). Magnesium fluoride (m.p. = 1,263 °C) is transparent over an extremely wide range of wavelengths, but its use in infrared screening is much appreciated. On the other hand, magnesium oxide (m.p. = 2,852 °C) is usually used as a colorimetric white reference, due to its good diffusion and reflection properties, and thus an excellent white emitter. More, its bright flame is persistent and it emits an important UV light.

It was observed that the PF-Mg (1 m) particle surface is more homogenous than the PF-Mg, presenting only one distribution maximum. This should be a consequence of the

Fig. 8 Distribution of the particles microspheres for PF-Mg and PF-Al aerosol samples taken from the combustion site and from 1 m away

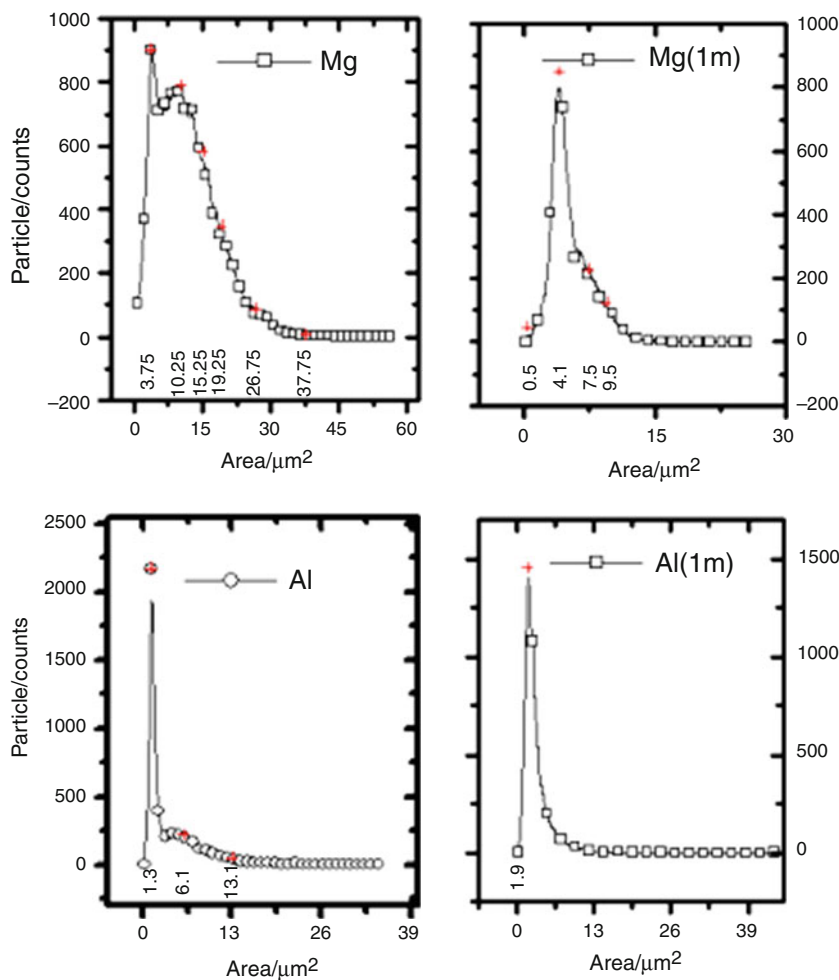
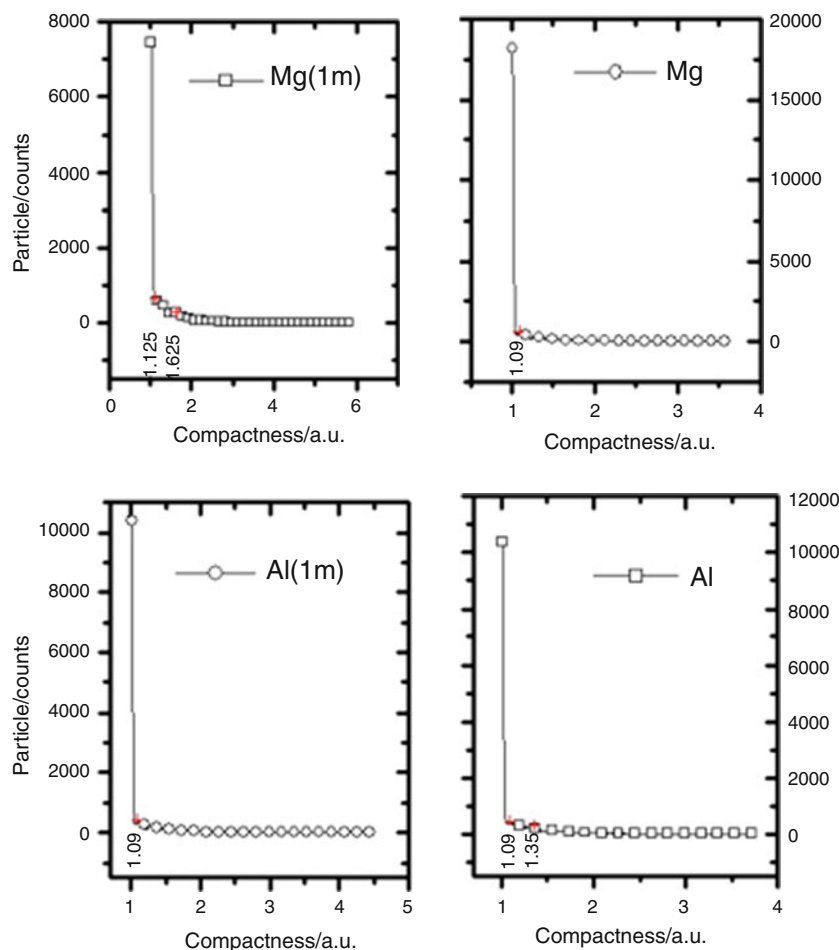


Fig. 9 Distribution of the particles compactness for PF–Mg and PF–Al aerosol samples taken from the combustion site and from 1 m away



existence of melted MgF_2 at the combustion site, and its diminishment while the flame is elongated. More, the numerical data recorded suggest that PF–Mg aerosols add up in larger agglomerations, with an irregular morphology of PF–Mg versus PF–Mg (1 m) (Table 3). It is very likely that PF–Mg (1 m) aerosols form agglomeration ranges as a consequence of elemental particles agglomeration.

PF–Al and PF–Al (1 m) aerosols present completely different morphostructures and dimensions; the experimental evidence from Figs. 8 and 9 demonstrates that these aerosols present mainly the same microsurface value. More, one may observe that PF–Al (1 m) versus PF–Al aerosols present a more emphasized tendency to form agglomeration ranges, with approximative values of 4.5, 6.9, 8.1, and $10.5 \mu\text{m}^2$. This evidence is confirmed by the numerical data recorded in case of PF–Al and PF–Al (1 m) samples compactness, which shows that the $[(P^2)/4DS]$ ratio (where: P —perimeter, D —particle diameter, and S —particle surface) is distributed in the range [1–3.72] in case of PF–Al, and is found at 4.42, in case of PF–Al (1 m).

EDX results proved that Al_2O_3 (amorphous oxide, m.p. = $2,072^\circ\text{C}$), elemental C, and AlF_3 are the main

Table 3 Area and compactness values and distribution ranges of aerosol samples

Sample	[Area/ μm^2] [compactness/a.u.]	[Area/ μm^2][compactness/ a.u.]agglomeration ranges
PF–Mg	[3.75, 8.75, 12.75, 15.25, 20.25][1.09]	[25.75, 29.25, 34.25][–]
PF–Al	[1.3][1.09]	[–][–]
PF–Mg (1 m)	[3.75][1.09, 1.35, 1.71]	[–][–]
PF–Al (1 m)	[1.3, 4.5, 6.9, 8.1, 10.5][1.09, 1.39, 1.81]	[4.5, 6.9, 8.1, 10.5] [1.39, 1.81]

solid products resulting from the combustion of PF–Al (Fig. 5b). Aluminum fluoride melts at $1,291^\circ\text{C}$ with sublimation, which conducts to the conclusion that more important quantities of aerosols are found away from the combustion site, the agglomeration sites being due to the mixture of the fluoride and the oxide. While the magnesium-based pyrotechnic composition considered tends not to spread far from the combustion site, the aluminum one offers a wider screening.

Conclusions

The combustion temperatures of the magnesium- and aluminum-based compositions are similar, reaching values close to 2,000 °C. However, the aluminum-containing composition proves better performances when considering both visible and infrared screening.

The experimental data processing using ImageJ software and the comparison of these data with the results obtained through direct measurement or processed with dedicated software concluded that the use of ImageJ software for the visible range gives a valuable output in processing images, regarding the screening efficiency and the corresponding parameters. The measurement of pyrotechnics combustion temperatures using optical pyrometers is quite easy and at the hand for temperatures up to 2,000 °C. The values obtained using the optical pyrometer and the thermal camera are different, due to the constructive limitations of the devices. The most accurate results in LWIR are obtained using the thermovision camera and processed with the dedicated software. Even though the thermal camera has an upper detection threshold lower than the pyrometer, its dedicated software allows the precise temperature determination, through mapping.

Acknowledgements The authors thank Professor Doru-Adrian Goga from Military Technical Academy of Bucharest and Senior Scientist Cătălin Spulber from SC PROOPTICA SA for the equipment made available during the tests performed and the fruitful discussions. This study has been supported by a Grant of the Romanian National Authority for Scientific Research, CNDI—UEFISCDI, Project No. 199/2012.

References

- Chrzanowski K. Testing thermal imagers. practical guidebook. Warsaw: Military University of Technology; 2010.
- Cudzilo S. Studies of IR-screening smoke clouds. *Propellants Explos Pyrotech.* 2001;26:12–6.
- Kang X, Zhang J, Zhang Q, Du K, Tang Y. Studies on ignition and afterburning processes of KClO_4/Mg pyrotechnics heated in air. *J Therm Anal Calorim.* 2012;109:1333–40.
- Goga DA. Pyrotechnics, basic principles and applications. Bucharest: Military Technical Academy; 2007.
- Conkling JA. Chemistry of pyrotechnics—basic principles and theory. New York: Marcel Dekker; 1995.
- Hosseini SG, Pourmortazavi SM, Hajimirsadeghi SS. Thermal decomposition of pyrotechnic mixtures containing sucrose with either potassium chlorate or potassium perchlorate. *Combust Flame.* 2005;141:322–6.
- Akhavan J. The chemistry of explosives. London: Royal Society of Chemistry; 1998.
- Fedorov AV, Shul'gin AV. Ignition and combustion of magnesium particles in a nonuniform thermal field. *Combust Explos Shock Wave.* 2009;45:151–9.
- Koch EC. Metal–fluorocarbon-pyrolants IV: thermochemical and combustion behaviour of magnesium/teflon/viton (MTV). *Propellants Explos Pyrotech.* 2002;27:340–51.
- Qu J, Duan H, Du X. Effect of aluminum powder on the luminous intensity of an illuminant. *Adv Mater Res.* 2012;512–515:2689–92.
- Pourmortazavi SM, Hajimirsadeghi SS, Kohsari I, Fathollahi M, Hosseini SG. Thermal decomposition of pyrotechnic mixtures containing either aluminum or magnesium powder as fuel. *Fuel.* 2008;87:244–51.
- Gillard P, De Izarra C, Roux M. Study of the radiation emitted during the combustion of pyrotechnic charges. Part II: characterization by fast visualization and spectroscopic measurements. *Propellants Explos Pyrotech.* 2002;27:80–7.
- Koch EC, Hahma A, Weiser V, Roth E, Knapp S. Metal–fluorocarbon pyrolants. XIII: high performance infrared decoy flare compositions based on MgB_2 and Mg_2Si and polytetrafluoroethylene/Viton®. *Propellants Explos Pyrotech.* 2012;37:432–8.
- Său C, Lăzăroaie C, Zecheru T, Petre R, Iordache PZ, Goga DA. Toxicity evaluation of smoke pyrotechnic compositions based on the dimensional analysis of solid combustion products. *Rev Chim.* 2011;62:718–22.
- Rotariu T, Zecheru T, Rusen E, Goga DA, Cincu C. Kinetic study of a new flame-retardant polymer composition. *Mat Plast.* 2011;48:83–7.
- Steinhauser G, Klapötke T. “Green” pyrotechnics: a chemists’ challenge. *Angew Chem Int Ed.* 2008;47:3330–47.
- Azhagurajan A, Selvakumar N, Thanulingam TL. Thermal and sensitivity analysis of nano aluminium powder for firework application. *J Therm Anal Calorim.* 2011;105:259–67.
- Zaharia C, Tudora MR, Miculescu F, Cincu C, Chappard D. Mineralization behaviour of some new phema-based copolymers with potential uses in tissue engineering. *Optoelectron Adv Mat.* 2011;5:314–7.
- Rugunanan RA, Brown ME. The use of pyrometry in the study of fast thermal processes involving initially solid samples. *J Therm Anal Calorim.* 1991;37:2125–41.
- Osborne DT, Pantoya ML. Effect of Al particle size on the thermal degradation of Al/teflon mixtures. *Combust Sci Technol.* 2007;179:1467–80.
- De Klerk WPC, Colpa W, Van Ekeren PJ. Ageing studies of magnesium–sodium nitrate pyrotechnic compositions. *J Therm Anal Calorim.* 2006;85:203–7.
- Vaulleir M, Morand P, Espagnacq A. Optimization of a smoke producer composition by experiment design. *Propellants Explos Pyrotech.* 2001;26:229–34.
- Zecheru T, Lungu A, Iordache PZ, Rotariu T. Thermal and spectroscopic measurements of some energetic compositions and corresponding aerosols obtained. *Combust Explos Shock Wave.* 2013;49(2):204–14.
- Barwood H. Digital near-infrared (NIR) cathodoluminescence (CL) imaging and image processing. *Am Mineral.* 2007;92:261–6.
- Kumar A, Negi YS, Bhardwaj NK, Choudhary V. Synthesis and characterization of methylcellulose/PVA based porous composite. *Carbohydr Polym.* 2012;88:1364–72.
- Borcan OV, Spulber C. An analytical approach regarding the choose of integration time and gain values during a thermal camera calibration. *Appl Mech Mater.* 2013;245:45–53.
- Mudau AE, Willers CJ, Griffith D, Le Roux FPJ. Non-uniformity correction and bad pixel replacement on LWIR and MWIR images. www.researchgate.net. Accessed 30 March 2013.
- FLIR Systems Inc., ThermaCAM Researcher Software. 2.8; 2004.
- Pellegrino JG, Zeibel J, Driggers RG, Perconti P. Infrared camera characterization. In: Diakides NA, Bronzino JD, editors. Medical infrared imaging. Boca Raton: CRC Press; 2008. p. 4–1–4–10.
- de Yong LV, Smit KJ. A theoretical study of the combustion of magnesium/teflon/viton pyrotechnic compositions. *MRL Technical Report MPL-TR-Qi-25.* Australia;1991. pp. 1–35.
- Iordache PZ, Lungu RM, Epure G, Mureşan M, Petre R, Petrea N, Pretorian A, Dionezie B, Mutihac L, Ordeanu V. The determination of the nanostructured materials’ morphology, by applying the statistics of the structural element maps. *J Optoelectron Adv Mater.* 2011;13:550–9.